Climate Dynamics (1997) 13: 167–180

Climate Dynamics

Can local linear stochastic theory explain sea surface temperature and salinity variability?

A. Hall*, **S. Manabe**

Princeton University, Atmospheric and Oceanic Sciences Program, Sayre Hall, Forrestal Campus, Princeton NJ 08544-0710, USA

Received: 11 March 1996 / Accepted: 6 September 1996

Abstract. Sea surface temperature (SST) and salinity (SSS) time series from four ocean weather stations and data from an integration of the GFDL coupled ocean-atmosphere model are analyzed to test the applicability of local linear stochastic theory to the mixed-layer ocean. According to this theory, mixed-layer variability away from coasts and fronts can be explained as a 'red noise' response to the 'white noise' forcing by atmospheric disturbances. At one weather station, Papa (northeast Pacific), this stochastic theory can be applied to both salinity and temperature, explaining the relative redness of the SSS spectrum. Similar results hold for a model grid point adjacent to Papa, where the relationships between atmospheric energy and water fluxes and actual changes in SST and SSS are what is expected from local linear stochastic theory. At the other weather stations, this theory cannot adequately explain mixed-layer variability. Two oceanic processes must be taken into account: at Panulirus (near Bermuda), mososcale eddies enhance the observed variability at high frequencies. At Mike and India (North Atlantic), variations in SST and SSS advection, indicated by the coherence and equal persistence of SST and SSS anomalies, contribute to much of the low frequency variability in the model and observations. To achieve a global perspective, TOPEX altimeter data and model results are used to identify regions of the ocean where these mechanisms of variability are important. Where mesoscale eddies are as energetic as at Panulirus, indicated by the TOPEX global distribution of sea level variability, one would expect enhanced variability on short time scales. In regions exhibiting signatures of variability similar to Mike and India, variations in SST and SSS advection should dominate at low frequencies. According to the model, this mode of variability is found in the circumpolar ocean and the northern North Atlantic, where it is associated with the irregular oscillations of the model's thermohaline circulation.

Correspondence to: A. Hall
e-mail: adh@gfdl.gov
* *Present address*: U.S. Department of Commerce/NOAA, Geophysical Fluid Dynamics Laboratory, P.O. Box 308, Princeton NJ 08542, USA

1 Introduction

Identifying the causes of natural variability in the climate system is a key challenge of present-day research. One theory, proposed by Hasselmann (1976), attempts to explain the mechanism of variability by dividing the climate system into fast and slow components. The atmosphere makes up the fast component, while the slow components include the ocean, cryosphere, and land surface. According to the best-known version of this theory, the variability of the slow components is explained as a linear response to random, white-noise forcing from the atmosphere. In this case, the localized response of the slow component, at a specified location at the sea surface, for example, can be described as a first-order Markov process: on short time scales, the slow component simply integrates atmospheric noise, while on longer time scales, this random-walk process is limited by linear negative feedback, or 'damping' which is proportional to the magnitude of the slow component anomaly.

Most applications have focused on the local, linear version of stochastic theory outlined above (abbreviated throughout the rest of this article simply as LLST for conciseness). Reynolds (1978) applied it to SST (sea surface temperature) anomalies in the North Pacific, using different statistical models to see where the SST spectrum can best be described as a red noise spectrum. Analyzing a simple ocean-atmosphere model and observations at weather station India, Frankignoul and Hasselmann (1977) examined LLST in the context of both SST anomalies and thermocline variability. Manabe and Stouffer (1996) assessed its relevance to SST variability by comparing results from coupled and mixed layer models. As in much of this previous work, the present study seeks to evaluate the appropriateness of LLST for the mixed layer ocean.

One main difference from previous research in this area is that our study examines the variability of sea surface salinity (SSS) as well as SST. This comparison of SST and SSS proves useful for two reasons. First, in oceanic regions where the mean current is small and random atmospheric forcing is the principal cause of mixed layer variability,

differences between the damping of SST and SSS anomalies should produce systematic differences in their spectra. SST anomalies are damped by sensible and latent heat and radiative fluxes across the air-sea interface as well as turbulent diffusion within the mixed layer, whereas SSS anomalies are damped by turbulent diffusion alone. Since SST anomalies are damped more effectively than SSS anomalies, a larger proportion of SSS variability ought to be concentrated at low frequencies. Thus in regions where LLST holds, the SSS spectrum ought to be redder than its SST counterpart. In regions where this is not the case, other mechanisms must be operating.

Secondly, comparison of SST and SSS is useful because oceanic processes that affect mixed-layer variability often have a distinctive signature which is difficult to discern through analysis of only one of the two parameters. For example, in the Gulf Stream or Kuroshio regions, the passage of saline, warm-core or fresh, cold-core eddies would introduce coherence between SST and SSS on short time scales. Conversely, large-scale variations in SST and SSS advection, which could be related to long-term changes in the North Atlantic thermohaline circulation, would lead to coherence on long time scales. Analysis of SST or SSS alone would not conclusively establish the presence of either one of these processes. This comparative analysis of SST and SSS therefore addresses two broad questions: First, is random forcing by atmospheric disturbances responsible for SST and SSS variability in accordance with LLST? And second, if LLST cannot explain this variability, then which oceanic processes can?

In order to answer these questions, time series of SST and SSS are analyzed using data from four ocean weather stations, whose geographical distribution (see Fig. 1) allows LLST to be tested in a wide range of oceanic settings. One (Papa) is located in the mid-latitude Pacific, another (Panulirus) is situated in the sub-tropical Atlantic, while the final two (Mike and India) are located in the mid to high latitudes of the Atlantic. These weather stations are among the very few locations in the world where both SST and SSS have been sampled continuously over a long time period.

In addition, SST and SSS data from a 1000-year integration of the GFDL coupled ocean-atmosphere model (Manabe and Stouffer 1996) are used to shed more light on the mechanisms of SST and SSS variability. For example, differences between the model and the observations may be attributable to physical processes not simulated by the model. On the other hand, similarities between the model and observations lend additional credence to the analysis. It should be emphasized, however, that even if the model includes all of the appropriate physical mechanisms, exact quantitative agreement between the observations and the closest model grid point is unlikely. With this caveat in mind, this study seeks broad-scale qualitative similarities between the model and observations as evidence that the same underlying physical mechanisms are at work in each realm. Finally, model data has the enormous advantage of coverage over the entire global ocean for an extended period of time. Once the limited observational record reveals the signatures of some important mechanisms of SST and SSS variability, the presence of these same signatures in model data can be used to extend the analysis to the entire world ocean, if only qualitatively.

2 Review of local linear stochastic theory

As a prelude to the results of the analysis given in Sect. 5, a brief outline of LLST and its extension to mixed-layer variability is presented below. As mentioned already, the main theoretical foundations of LLST were laid out by Hasselmann (1976). However, in the context of this study, it is necessary to clarify the circumstances under which the linear, local version of this theory may be applied to SST and SSS anomalies. In addition, it is important to identify precisely the expected differences in the behavior of SST and SSS when LLST is applicable. In order to accomplish these goals, we begin with an equation of mixed-layer variability that includes the effects of horizontal advection

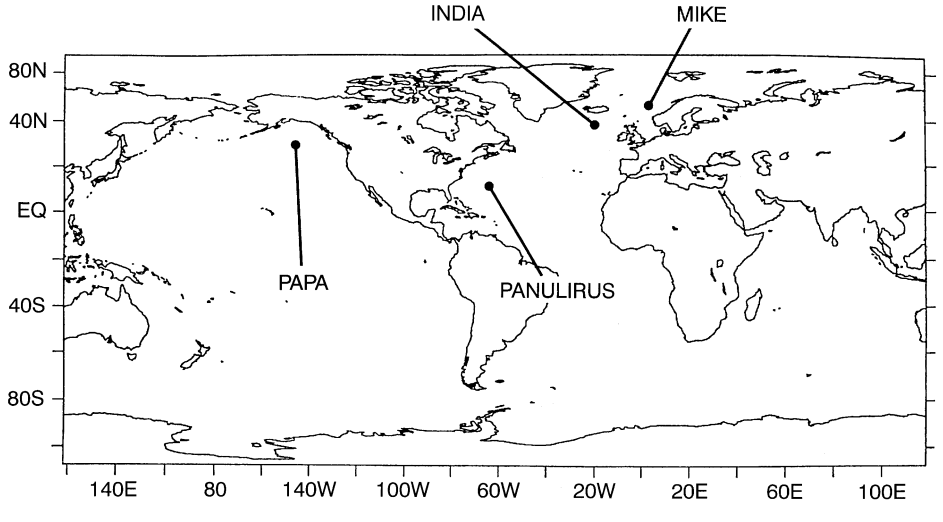

Fig. 1. The locations of the weather stations used in the analysis

and atmospheric forcing and reduce it to the familiar Langevin equation:

$$ch\frac{\partial \Theta'}{\partial t} = \xi' - ch(v_2 \cdot \nabla_2 \Theta)' \tag{1}$$

The derivative on the left hand side represents the local time tendency of the mixed-layer anomaly Θ', which could represent either a temperature or a salinity anomaly. It is multiplied by the depth of the mixed layer, h, and the 'capacity' of the water column, c, giving the left-hand side the units of a flux per unit area of surface ocean. In the case of temperature, this 'capacity' is simply the heat capacity of seawater. However, for salinity, it is the reciprocal of the time-averaged salinity of the mixed layer. On the right hand side, ξ' represents the anomalous flux across the air-sea interface. In the case of temperature this is an energy (sensible and latent heat plus radiative) flux per unit area, while for salinity, it is a water (evaporation minus precipitation) flux per unit area. The second term represents the effects of anomalous horizontal advection. This scheme therefore neglects oceanic processes such as deep convection, downwelling and upwelling, all of which can generate SST or SSS anomalies independently of air-sea fluxes of heat and water. Strictly speaking, a passive ocean responding only to atmospheric forcing requires the elimination of the horizontal advection term as well. Certainly in regions where large-scale variations in the ocean circulation produce variability in SST and SSS advection, or where mesoscale eddies induce salinity and temperature anomalies, this term represents an important source of forcing. In these regions LLST cannot adequately explain the variability. However, in regions of the ocean where the mean current is small (i.e. $\bar{v} \approx 0$) and there is very little mesoscale eddy activity, this term may be regarded as a representation of small-scale turbulent diffusive processes, which act to damp anomalies back to the mean. Then to a first order approximation, this diffusive damping is proportional to the negative of the temperature or salinity anomaly. This is admittedly a crude approximation, neglecting mainly the fact that diffusive damping ought to be scale-selective, operating most effectively on anomalies that are small in spatial extent. However, replacing the horizontal advection term with a linear damping term representing negative feedback does capture the essence of the effects of diffusion and simplifies the mathematics considerably:

$$C\frac{\partial \Theta'}{\partial t} = \xi' - \lambda_d \Theta' \tag{2}$$

Here $C = ch$, and λ_d is the constant of proportionality relating the magnitude of the mixed layer anomaly to the time rate of change of that anomaly due to diffusion. Turbulent diffusion is the only oceanic process that may be reasonably represented as a damping term, since other advective processes, such as large-scale SST and SSS advection by ocean currents or mesoscale eddy activity, generate anomalies rather than damp them.

Equation (2) shows how LLST would model the evolution of SSS anomalies. However, in the case of temperature, there is an additional consideration. In contrast to the surface water flux, which is not directly affected by SSS anomalies, the energy flux across the air-sea interface is determined not only by atmospheric conditions but also by the temperature of the ocean surface. There is a component of the flux that is proportional to the negative of the mixed-layer temperature anomaly. This component can be represented using a damping term as in Eq. (2). The remaining flux, the atmospheric force, is denoted by the symbol η'. Using the symbol λ_a to identify the component of the damping due to atmospheric feedback and letting $\xi' = \eta' - \lambda_a \Theta'$, Eq. (2) becomes:

$$C\frac{\partial \Theta'}{\partial t} = \eta' - (\lambda_a + \lambda_d)\Theta' \tag{3}$$

Comparing Eqs. (2) and (3), we see that Eq. (3), representing the evolution of SST anomalies, reduces to its SSS equivalent (2) if we let $\lambda_a = 0$ and $\eta' = \xi'$; SSS anomalies are damped by diffusion alone. If diffusion were not included in LLST, the ocean would act as a simple integrator of atmospheric noise. This would produce a random walk process in SSS, with variance increasing in time, which is clearly unphysical. Any formulation of LLST for the mixed layer must therefore include diffusive processes in the damping term. Since turbulent diffusion ought to affect temperature and salinity equally, we expect the total damping to be larger for SST than for SSS.

Letting $\lambda = \lambda_a + \lambda_d$, Eq. (3) can be used to derive a spectrum of Θ':

$$|\tilde{\Theta}'(\omega)|^2 = \frac{\left|\frac{\tilde{\eta}(\omega)}{C}\right|^2}{\omega^2 + \left(\frac{\lambda}{C}\right)^2} \tag{4}$$

The term on the left side of Eq. (4) represents the power spectral density of either temperature or salinity, which is given in terms of λ, C, the power spectral density of the atmospheric forcing, $|\tilde{\eta}(\omega)|^2$, and the angular frequency, ω. If the atmospheric forcing is a random, white noise process, as is generally assumed in LLST, then its power spectral density will be a constant function of frequency. From an oceanic point of view, white noise atmospheric forcing is probably a good assumption over most of the world ocean, since the rapid passage of synoptic disturbances results in an autocorrelation time scale of just a few days for the atmosphere. This is much shorter than typical time scales of mixed layer variability. In the case that the white noise forcing assumption does hold, it becomes clear from Eq. (4) that there are two regimes of interest: At high frequencies, when $\omega \gg \lambda/C$, the response spectrum falls off as $1/\omega^2$. This is characteristic of a random-walk process. Conversely, at low frequencies, when $\omega \ll \lambda/C$, the spectrum will be independent of frequency, depending only on λ. Thus the value of λ/C determines the 'bending point', i.e. the frequency at which the spectrum passes from one regime to the other. Since we expect λ/C to be larger for temperature than for salinity, the bending point in the salinity spectrum ought to come at a lower frequency, producing a spectrum that is 'redder' than its temperature

counterpart. In regions where the local, linear stochastic mechanism operates, spectral analysis of both SST and SSS should reveal this signature.

Based on this discussion, LLST is most applicable in regions of the ocean where the mean current is very small and turbulent diffusion is the dominant oceanic process. In regions where there is significant large-scale oceanic advection of SST and SSS, mesoscale eddy activity, upwelling, downwelling, or deep convection, one would not expect LLST to explain adequately mixed-layer variability.

3 Diagnostic procedures

Ocean weather stations were selected according to two criteria. First, it was desirable to have as long a time series as possible, with high sampling rates to minimize aliasing. Second, as mentioned in Sect. 1, it was desirable to test LLST in as wide a variety of oceanic settings as possible. The four weather stations that best meet these criteria for both temperature and salinity are Papa (50 °N, 145 °W), Panulirus (32 °10′N, 64 °30′W), Mike (66 °N, 2 °E) and India (59 °N, 19 °W). Their locations are shown in Fig. 1. The data from the three Atlantic stations were obtained from Dr. Gilles Reverdin, of Lamont-Doherty Laboratory. Salinity data at station Papa were obtained from the National Oceanographic Data Service (NODC) and the Marine Environmental Data Service (MEDS) of Canada, while SST data at this location were provided both by MEDS and the National Climatic Data Service (NCDC).

In order to isolate temporal from spatial variability, all data taken at locations further than 15 km from the official location of each weather station were removed. The remaining data were corrected for the displacement of a ship from its official location using the climatological spatial gradients according to Levitus (1982). In general, these corrections were very small, owing both to the stringency of the 15 km criterion and the fact that the bulk of the data was taken much closer to the official location than 15 km.

Since the focus of this study is variability, the component of the seasonal cycle that does not vary from year to year was removed. After constructing a time series of monthly averages from the raw data, a standard way to accomplish this task is to create a composite seasonal cycle of twelve data points by averaging the monthly means corresponding to each calendar month. The differences between these twelve data points and their mean constitute seasonal 'corrections' that are applied to each monthly average according to its position in the annual cycle. However, because the observational data were inhomogeneously sampled in time, this technique is not adequate for this study, as the following example illustrates. If in a given year, April SST measurements were taken only during the beginning of the month, the resulting monthly average would not be representative of the evolution of SST throughout April. Since the ocean in the Northern Hemisphere warms at this time of year, applying the April seasonal correction to this monthly mean would assume that more seasonal warming had taken place than actually occurs by the beginning of April. The adjusted monthly mean would be artificially cool owing to the overcorrection.

In order to address this issue, a different technique was used. First, a 12-point composite seasonal cycle was constructed by averaging the monthly means corresponding to each calendar month. In order to convert this composite cycle to one that varies continuously throughout the year, its Fourier transform was taken. This produced sine and cosine components that were added together to give a smoothly varying composite cycle. This continuous cycle could then be sampled at any time of the year, providing a seasonal adjustment for each raw data point according to its exact position in the annual cycle. Monthly means were calculated from these seasonally adjusted data, producing the final time series for statistical analysis. Obviously, the model's monthly means do not suffer from inhomogeneous sampling; thus the more standard technique was used to remove the seasonal cycle from model data.

Both spectral and cross-spectral statistics were used in the analysis. The spectral statistics were calculated using the lag autocovariance method, where the power spectrum is calculated by taking the cosine transform of the autocovariance function. Normalized spectra were also calculated by taking the cosine transform of the autocorrelation, rather than the autocovariance, function. Since the variances of the time series are constrained to be equal in the normalized case, the redness of the SST and SSS spectra may be easily compared. The cross-spectral statistics were calculated by taking the sine and cosine transforms of the cross-covariance function to give the quadrature and co-spectra, respectively. Gaps in the time series were treated in the following way: if covariances between two different points in time involved missing data at either or both points, that covariance was not included in the calculation of the autocovariance function. The same technique was used in the calculation of the cross-covariance function.

4 The coupled model

4.1 Model structure

This model is described in some detail in Manabe et al. (1991). It consists of a general circulation model of the world ocean coupled to an atmospheric general circulation model through exchange of heat, water, and momentum. The model includes all of the features of the Earth's geography that its resolution permits. It also has a seasonal cycle of insolation, although the diurnal cycle is not included.

The variables of the atmospheric component are represented in the horizontal by a series of spherical harmonics. Fifteen zonal waves and associated Legendre functions are included in the integration (Orszag 1970; Gordon and Stern 1982). In the vertical, finite differencing is used at nine unevenly spaced levels. The radiative transfer calculation includes the effects of clouds, water vapor, carbon

dioxide, and ozone on both incoming and outgoing radiation. The sky is overcast whenever the relative humidity exceeds 99%, otherwise clear sky is predicted. While the distribution of water vapor is predicted by the model, carbon dioxide concentration is taken to be constant. Ozone is specified as a function of latitude, height and time of year, following observations. At the land surface, the model computes budgets of snow, water, and heat based on the fluxes determined by the simulated atmospheric circulation. Manabe and Hahn (1981) carried out a general evaluation of the realism of the atmospheric variability of the model. They showed that the geographical distribution and magnitude of the standard deviation of 1000 mb geopotential height agrees well between model and observations (see Fig. 5.1–5.8 of that paper). This indicates that the model does reasonably well in simulating synoptic-scale weather disturbances, the main source of stochastic forcing for the ocean.

The finite-difference oceanic component, with a horizontal resolution of 3.75° latitude by 4.5° longitude and 12 vertical levels, is similar to the model described by Bryan and Lewis (1979). In addition to horizontal and vertical background sub-grid scale mixing, the model has isopycnal mixing as discussed by Redi (1982) and Tziperman and Bryan (1993). Convection occurs whenever the vertical stratification becomes unstable. Sea ice is predicted using a free drift model developed by Bryan (1969).

4.2 Time integration

At the beginning of time integration, the model's atmosphere and ocean are both individually in equilibrium with realistic seasonal and geographical distributions of SST, SSS, and sea ice. However, as the integration proceeds, the model's climate usually drifts toward its own, less realistic equilibrium state. This distorts the simulated natural variability that this study seeks to diagnose. To minimize this drift, the fluxes of heat and water obtained from the atmospheric component of the coupled model are modified by given amounts before they are imposed upon the ocean surface. While these adjustments vary seasonally and geographically, they do not vary from year to year. Moreover, these adjustments are determined prior to the coupled integration itself; they therefore are not correlated to the transient SST and SSS anomalies that develop over the course of the coupled integration. Thus, in contrast to the strong damping of SST and SSS anomalies when surface conditions are relaxed back to observed values as an ocean-only model is integrated, flux adjustment is unlikely to either systematically amplify or damp SST and SSS anomalies. Although the adjustments do not eliminate the shortcomings of the model (Marotzke and Stone 1995), they do prevent rapid drift of the simulated climate from realistic initial conditions.

Using this technique, the model was integrated for 1000 years, producing monthly averages of SST and SSS (see Manabe and Stouffer 1996 for further details of the integration). Five hundred years of data, comprising the last half of this time series, were used for the present analysis.

5 Time series analysis

5.1 Papa

As illustrated in Sect. 1, the local, linear stochastic mechanism requires a relatively passive ocean. The conditions at weather station Papa, which lies some 800 miles off the coast of Canada in the northeast Pacific, are well-suited to this requirement. It is a relatively inactive region of the world ocean. The annual mean current is small (about 4 cm/s in the real ocean, according to ship drift data, and about 0.4 cm/s in the model) and there is almost no upwelling (Oort et al. 1994).

The results of spectral analysis are consistent with the local, linear stochastic picture. Shown in Fig. 2 are the normalized spectra of SST and SSS for the observations and a model grid point adjacent to Papa. In the case of the observations, both spectra are consistent with a $1/\omega^2$ dependence at high frequencies, while at low frequencies, the spectra bend to a constant value, as expected from LLST. Furthermore, the SSS spectrum is redder than its SST counterpart. This is indicated by the fact that the bending point comes at a lower frequency for SSS, and by the way in which SSS has a much higher proportion of its variance concentrated at low frequencies. The slightly enhanced variability of SST on very short time scales is attributable to aliasing. At the high frequency end of the SSS spectrum, there is a dip, followed by a small peak. These are probably spurious, both because the variance in this frequency band is so small to begin with and because of gaps in the salinity time series. These factors make the spectral estimate less reliable on short time scales. The damping coefficient, λ/C, can also be calculated by performing a least squares fit to the logarithm of the autocovariance function. For salinity, $\lambda/C = (11.6 \text{ months})^{-1}$, while for temperature, $\lambda/C = (4.3 \text{ months})^{-1}$. For the sake of completeness and comparison with results presented in other sections of this article, the coherency between SST and SSS is shown in Fig. 3. Coherency is a statistic that quantifies the relationship between two time series at various time scales and is analogous to the square of the usual correlation coefficient. At nearly all frequencies, the coherency line below the horizontal dashed line, where 95% of the points would lie if the two time series were incoherent. This indicates that there is no significant coherency between SST and SSS at weather station Papa. Assuming the heat and water fluxes across the air-sea interface fluctuate incoherently, this result is also consistent with LLST.

Qualitatively similar results are found for the model grid point adjacent to Papa; SSS is redder than SST, and the shapes of the spectra are similar to what LLST predicts, indicating that the local, linear stochastic mechanism may be at work in the model as well. Quantitative agreement between model and observations, not surprisingly, is lacking. As the figure caption indicates, the total variances of SST and SSS are different from the observations, especially in the case of salinity. In addition, the model spectra are much redder than their observational counterparts. Thus, the values of the damping coefficients are smaller: $\lambda/C = (28.2 \text{ months})^{-1}$ for salinity while for temperature, $\lambda/C = (5.7 \text{ months})^{-1}$. This difference in

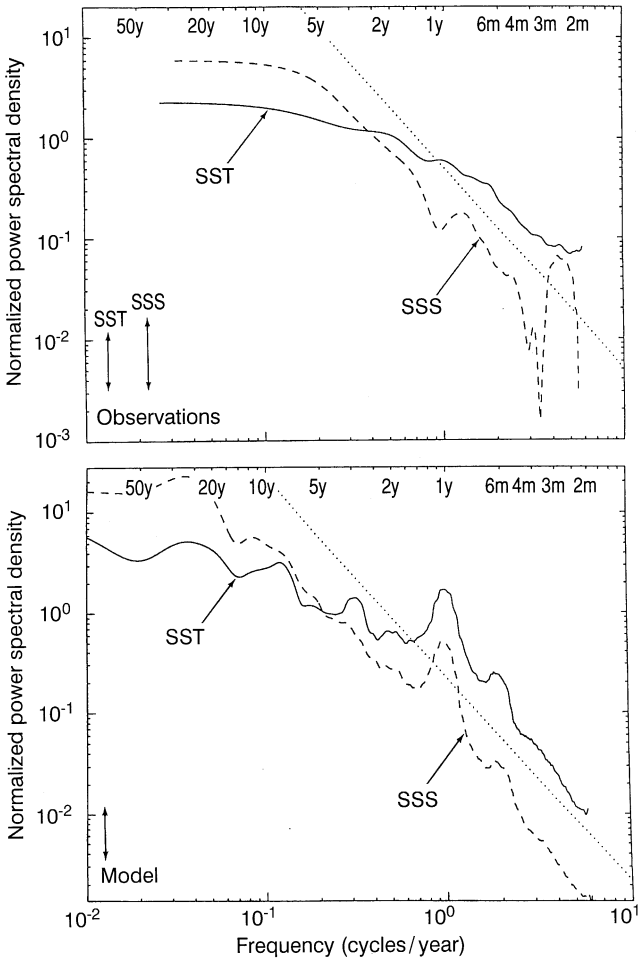

Fig. 2. *Top*: the normalized spectra of SSS (*dashed*) and SST (*solid*) at weather station Papa. The spectra were calculated by taking the Fourier transform of the autocorrelation function using a Parzen window with a maximum lag of 6 y. They were then smoothed by equal weighted averaging over a base 10 logarithmic frequency interval of 0.15. The total variances used to normalize the autocovariance function were 0.00960 psu^2 for SSS and 0.616 (°C)^2 for SST. The spectra are plotted out to the length of the time series (37.9 y for SST, 31.25 y for SSS). *Bottom*: the normalized spectra of SSS (*dashed*) and SST (*solid*) at a model grid point adjacent to weather station Papa (51.8 °N, 148.1 °W). The spectra were calculated by taking the Fourier transform of the autocorrelation function using a Parzen window with a maximum lag of 70 y. They were then smoothed by equal weighted averaging over a base 10 logarithmic frequency interval of 0.10. The total variances used to normalize the autocovariance function were 0.0733 psu^2 for SSS and 0.712 (°C)^2 for SST. The *dotted lines* show the characteristic $1/\omega^2$ slope. Time scales are shown on the upper edges of the plots. The *arrows* in the lower left corners indicate the 95% confidence intervals for the longest time scales, although the confidence intervals become smaller as frequency increases owing to the smoothing of the spectra. In the lower plot, the spectral peak at one year arises because the amplitude of the annual cycle varies a great deal from year to year at this grid point. Thus removing a composite seasonal cycle that does not vary from year to year, as discussed in Sect. 3, still leaves a residual annual signal

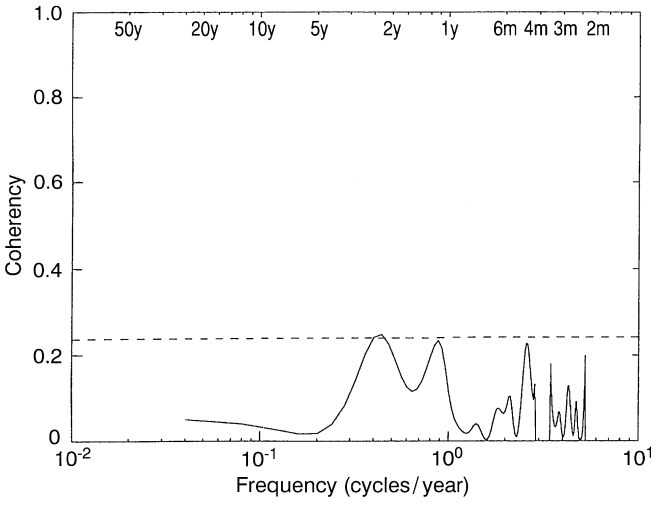

Fig. 3. The coherency between SST and SSS at weather station Papa. The *dashed horizontal line* shows the threshold below which 95% of the points would lie if the two time series were incoherent, as calculated according to the formula given by Julian (1975). Time scales are shown on the upper edge of the plot. The cross spectral statistics were calculated by taking the Fourier transform of the cross-covariance function using a Parzen window with a maximum lag of 40 months

redness may be due to the fact that the model ocean is represented by a finite difference grid in the vertical as well as the horizontal direction. The depth of the model mixed-layer cannot be smaller than 50 m, which is the depth of the topmost layer resolved by the model. Of course, wintertime convection may increase the penetration of the mixed layer to deeper grid points, but in summertime, the mixed layer is fixed at 50 m. In the real world, on the other hand, the depth of the mixed layer may be substantially less than 50 m during the warm months at mid-latitudes. In fact, at Papa, the mixed layer depth is less than 50 m for approximately 4.5 months per year (Alexander and Penland 1996). During this period, C is relatively small, making λ/C relatively large. In addition, even in wintertime, it is unlikely that the climatological penetration depth of convection will be the same in the model as in the real world for any particular location. It may be that the model's effective mixed-layer depth is larger in the winter as well as the summer. Yet another explanation for the difference in redness may lie in the fact that the observational record, unlike the model, has anomalies smaller in scale than a model grid box. This seems reasonable because air temperature, precipitation and evaporation in the real world can vary on spatial scales of the order of tens of kilometers, whereas the size of a grid box is of the order of hundreds of kilometers. Since diffusion damps smaller scale anomalies more effectively, these sub-grid scale anomalies may have shorter lifetimes than the model's anomalies simply because of their smaller scale. This difference between the model and real world will affect the damping of both temperature and salinity anomalies, but it will be more noticeable in the case of salinity, since a large proportion of the damping of SST anomalies is accomplished through atmospheric feedback. In fact, the discrepancy between model and observational damping coefficients is indeed larger for salinity than temperature, suggesting that this explanation may be relevant.

Verifying that the atmospheric forcing is white noise and causes sea surface variability is difficult for the

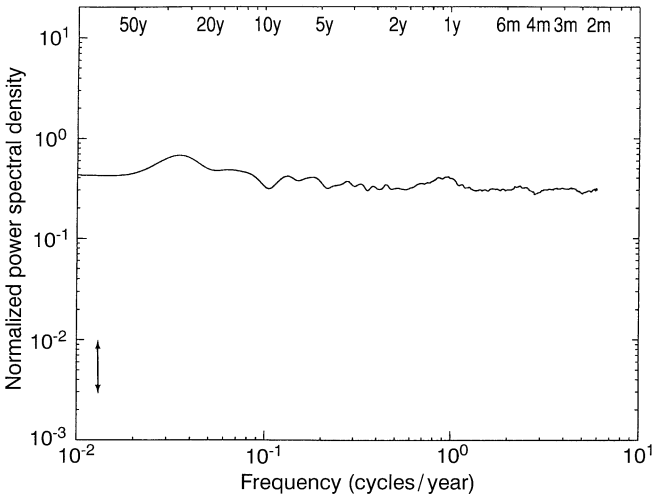

Fig. 4. The normalized spectrum of the water flux at the model grid point adjacent to weather station Papa. The spectrum was calculated by taking the Fourier transform of the autocorrelation function using a Parzen window with a maximum lag of 70 y. It was then smoothed by equal weighted averaging over a base 10 logarithmic frequency interval of 0.10. The total variance used to normalize the autocovariance function was 0.0183 (cm/day) ^{2}. Time scales are shown on the upper edge of the plot. The *arrow* in the lower left corner indicates the 95% confidence interval for the longest time scales, as in Fig. 2

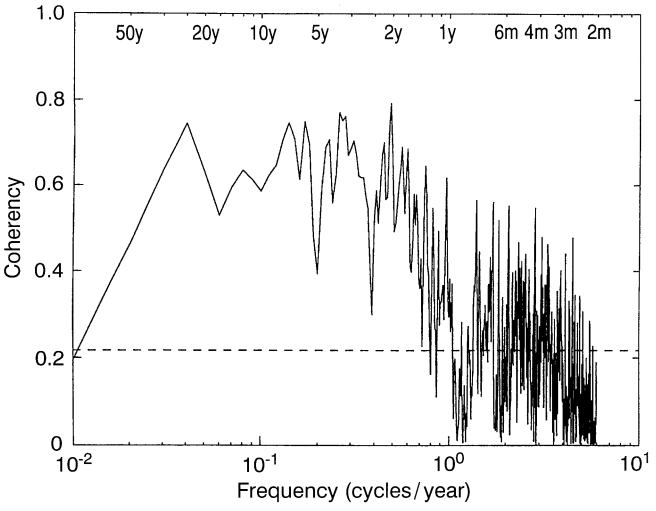

Fig. 5. The coherency between the water flux anomalies and salinity's residual noise time series at the grid point adjacent to Papa. The *dashed horizontal line* shows the threshold below which 95% of the points would lie if the two time series were incoherent, as calculated according to the formula given by Julian (1975). Time scales are shown on the upper edge of the plot. The cross spectral statistics were calculated by taking the Fourier transform of the cross-covariance function using a Parzen window with a maximum lag of 70 y

observations, since it involves constructing a time series of energy and water fluxes at the atmosphere-ocean interface. However, using model data alone, it is possible to carry out such an analysis. In the case of SSS, the white noise forcing assumption may be tested by calculating a normalized spectrum of the total water flux across the air-sea interface for the grid point adjacent to Papa, shown in Fig. 4. Spectral density is nearly independent of frequency, indicating that the spectrum of water flux can be characterized as white in this frequency band. However, this result does not prove that atmospheric forcing is responsible for SSS variability. In order to address this question it is necessary to demonstrate a causal relationship between water flux anomalies and the month-to-month changes in SSS.

This task was accomplished by inserting the model's month-to-month salinity anomalies and the calculated value of λ/C into a finite difference form of Eq. (3) and then solving for a time series of the forcing term, η'. An identical procedure was carried out for model SST. These time series, referred to hereafter as 'residual noise time series', were then analyzed using the coherency statistic. Although analogous to the square of the usual correlation coefficient, as mentioned already, coherency has an advantage over the correlation coefficient in that it can detect phase differences between fluctuations that are closely related and therefore highly coherent but consistently out of phase. Figure 5 shows the coherency between the water flux anomaly time series and the residual noise time series for salinity, which is effectively a history of the forcing required to produce the model's changes in salinity at this location. The coherency rises above the 95% confidence threshold at nearly all time scales. In addition, the phase difference between the two time series (not shown) indicates that the water flux at this location varies in phase with changes in salinity. These results demonstrate that a major fraction of fluctuations in salinity is determined by the water flux across the air-sea interface. However, while the coherency is high from time scales of 50 years to 1 year, it is never identically equal to one, suggesting that other processes may have some influence on salinity at this grid point. Perhaps the current is advecting small-scale, relatively short-lived anomalies from neighboring grid points, explaining the relatively low coherency on short time scales.

If LLST is applicable to SSS variability at this grid point, it is likely to apply SST variability as well. However, the analysis of the coherency between the energy flux anomaly time series, Q', and the residual noise time series for temperature, shown in Fig. 6, is more complex, since both forcing and damping are included in the net energy flux across the atmosphere-ocean interface, as indicated by Eq. (3). A simple scaling argument applied to that equation illustrates how to interpret Fig. 6: on time scales much longer than the damping time scale, the atmosphere and the ocean are essentially in equilibrium. This makes the total energy flux across the air-sea interface ($Q' = \eta' - \lambda_a \Theta'$) small compared to its individual forcing (η') and damping ($\lambda_a \Theta'$) components, which therefore tend to be equal and opposite. However, if the atmosphere is the sole source of forcing, the mixed layer must always obey the thermodynamical constraint that $Q' = C\partial\Theta'/\partial t$. Therefore, on long time scales, finding the coherency between the residual noise time series, $\eta'(\approx \lambda_a \Theta')$, and the energy flux anomaly time series, Q', is tantamount to finding the coherency between the damping term, $\lambda_a \Theta'$,

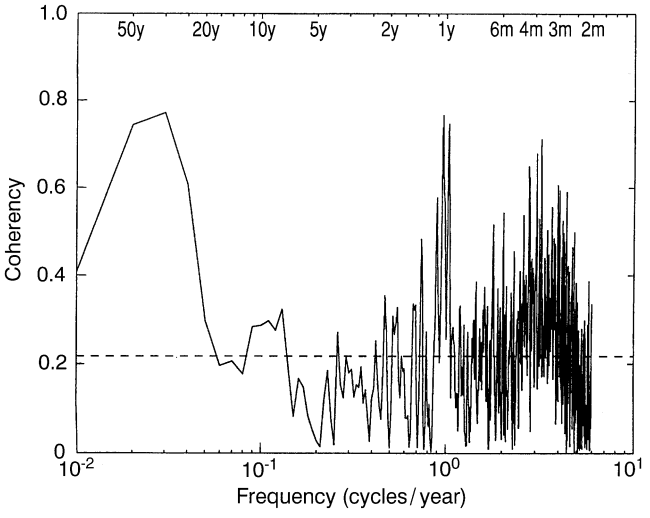

Fig. 6. The coherency between the total energy flux anomalies (radiative + sensible + latent) and temperature's residual noise time series at the grid point adjacent to Papa. The *dashed horizontal line* shows the threshold below which 95% of the points would lie if the two time series were incoherent. Time scales are shown on the upper edge of the plot. The cross spectral statistics were calculated by taking the Fourier transform of the cross-covariance function using a Parzen window with a maximum lag of 70 y

and the time derivative of the temperature anomaly, $C\partial\Theta'/\partial t$. These latter two quantities ought to be coherent with a 90° phase lag between them. Conversely, on time scales much shorter than the damping time scale, the damping terms of Eq. (3) are small compared to the other terms, making the atmospheric forcing the dominant component of the air-sea flux. Thus on very short time scales, if LLST is applicable, the total energy flux anomalies should be coherent, and in phase with, changes in SST. At intermediate time scales, neither one of these relationships may hold, giving relatively low coherence between the flux anomaly and residual noise time series.

These points are well illustrated by Fig. 6, which shows the coherency between the total energy flux anomalies and the residual noise time series for SST. On time scales longer than 20 years, the two time series fluctuate coherently with a phase lag of about 75° (phase lag plot not shown). The phase lag may be less than 90° because diffusion also plays a role in the damping of SST anomalies. (The argument presented above assumed that $\lambda_d\Theta'$ is negligible compared to $\lambda_a\Theta'$). At intermediate time scales (20 years to one year), the coherency in general is quite low, although some peaks do rise above the 95% confidence threshold. Finally, at time scales shorter than a year, the coherency again becomes high, and the phase difference between the two time series indicates that the energy flux does vary in phase with changes in temperature, as expected.

Together, all of these model results provide compelling evidence of the validity of LLST at this grid point. The SSS spectrum is redder than its SST counterpart and both spectra agree reasonably well with a red noise spectrum. By themselves, these results are merely consistent with the local, linear stochastic picture. However, LLST can only be proven if it can be shown that white noise atmospheric forcing causes the variability in the mixed layer. Together, Figs 4, 5 and 6 provide support for this crucial assumption.

5.2 *Panulirus*

Figure 7 shows the spectra of SST and SSS at weather station Panulirus, near Bermuda in the North Atlantic, for the model and observations. These spectra were calculated by taking the cosine transform of the autocovariance function, so that absolute comparisons of variance between model and observations can be made at different time scales. Unlike the model, the SST and SSS observations fail to exhibit the characteristic $1/\omega^2$ dependence at high frequencies. Thus the shapes of the observational spectra are qualitatively different from the model spectra. Moreover, while the levels of variance of the model and observation spectra are comparable on time scales longer than one year, the variance of the observations is an order of magnitude larger than that of the model on short time scales. This is true for both SST and SSS. This result is similar in spirit to the work of Frankignoul (1981), who compared the SST spectrum at Panulirus to the spectrum of observed SST fluctuations averaged over a $5^\circ \times 5^\circ$ box containing the Bermuda region. That study found that the former had substantially higher variance at periods less than one year than the latter. Since temporal and spatial scales tend to be correlated in the atmosphere and ocean, these results indicate that a dynamical process not resolved by the model (or filtered out by spatial averaging, in the case of the observations) may be responsible for the enhanced variability on short time scales.

One important sub-grid scale process is mesoscale eddy activity. Recently, the availability of TOPEX altimeter data has made it possible to measure the sea level variability at nearly all locations of the world ocean. Although not a precise measure of mesoscale eddy activity, since sea level changes do not fully reflect the eddies' baroclinic component, regions of high sea level variability nevertheless tend to coincide with regions where eddies are particularly active. According to a map showing the geographical distribution of sea level variability (see Fig. 8), Panulirus lies just at the southern fringes of a region of high sea level variability (rms variability $\geqslant$12 cm) associated with the mesoscale eddies of the Gulf Stream. The Gulf Stream separates warm, saline water to the south from cold, fresher water to the north; and it is well known that the eddies it produces are characterized by the origin of the water they contain. Thus, 'warm core' eddies are composed of saline water from the subtropics, whereas 'cold core' eddies contain fresher water from the mid latitudes (Robinson 1983). The passage of eddies should therefore be discernible through comparison of the temperature and salinity record at a given location. In particular, SST and SSS ought to be coherent on time scales typical of eddy activity, which range from a few weeks to a few months. Of course, the signature of the very highest frequency eddies would not be present in this particular record, since the construction of monthly averages acts as a low pass filter.

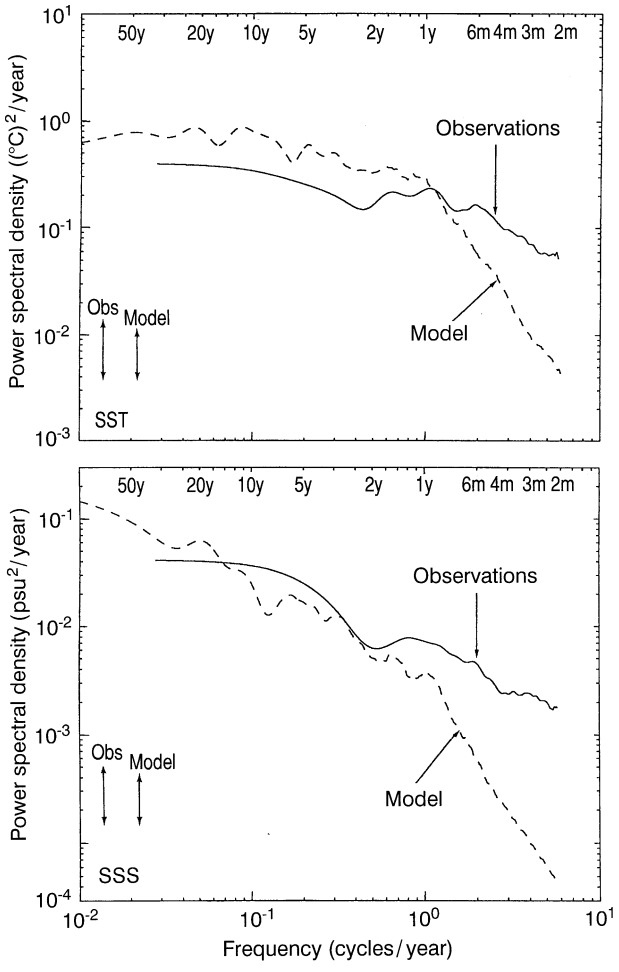

Fig. 7. *Top*: the spectra of SST at weather station Panulirus (*solid*) and the nearest model grid point at 33.8 °N, 65.6 °W (*dashed*). *Bottom*: the spectra of SSS at weather station Panulirus (*solid*) and the nearest model grid point (*dashed*). The observational spectra were calculated by taking the Fourier transform of the autocovariance function using a Parzen window with a maximum lag of 6 y. They were then smoothed by equal weighted averaging over a base 10 logarithmic frequency interval of 0.15. The model spectra were calculated by taking the Fourier transform of the autocovariance function using a Parzen window with a maximum lag of 70 y. They were then smoothed by equal weighted averaging over a base 10 logarithmic frequency interval of 0.10. The observational spectra are plotted out to the length of the time series (36.6 y for both SST and SSS). Time scales are shown on the upper edges of the plots. The *arrows* in the lower left corners indicate the 95% confidence interval for the longest time scales, as in Fig. 2

To determine if mesoscale eddy activity is responsible for the observed enhanced variability on time scales shorter than one year, the coherency of SST and SSS at Panulirus was calculated, and is shown in Fig. 9. Unlike weather station Papa, which exhibits no significant coherency between SST and SSS on any time scale, at Panulirus there is a broad band of coherency on time scales shorter than one year, with several of the peaks rising well above the 95% confidence threshold. This, along with the altimeter data, provides compelling evidence that mesoscale eddies make significant contributions to the SST and SSS variability at Panulirus. Figure 9 also illustrates how joint analysis of SSS as well as SST can reveal the main mechanisms of variability in a very simple way.

The conclusion that mesoscale eddies are a significant source of variability at Panulirus is consistent with the work of Frankignoul (1981), who showed that the vertical structure of temperature variability at Panulirus closely resembles the first two eddy baroclinic modes. Thus in the case of Panulirus, the advection term in Eq. (1) cannot be reduced to a simple turbulent diffusion term. It also represents eddy activity, which pushes SST and SSS away from the mean and therefore is properly thought of as a forcing rather than a damping mechanism. In spite of the fact that the annual mean current is very small at Panulirus (on the order of 1.5 cm/s, according to ship drift data), oceanographic processes make an important contribution to SST and SSS variability. Since the atmosphere is not the only source of forcing at Panulirus, LLST is not adequate to explain the observed variability. This is clearly the case on short time scales, although LLST may be more applicable at low frequencies. In fact, close inspection of Fig. 7 shows that the observed SSS spectrum is redder than its SST counterpart. On spatial and temporal scales much larger than the eddies, atmospheric forcing and the enhanced damping of SST relative to SSS may be operating in this region. In this way, the local, linear stochastic mechanism may work in tandem with mesoscale eddies to produce the observed signature of variability.

5.3 Mike and India

Figures 10 and 11 show the normalized spectra of SST and SSS at weather stations Mike and India and their nearest model grid points. Both weather stations are located in the North Atlantic. As in the analysis for Papa, these spectra were calculated by taking the cosine transform of the autocorrelation function, allowing for comparisons of the redness of SST and SSS. Although the observational spectra at India are somewhat flatter than the characteristic $1/\omega^2$ at high frequencies, a perfect red noise spectrum is not an unreasonable fit for all of the observed spectra. In fact, Frankignoul and Hasselmann (1977) interpreted the goodness of the red noise fit to the observed SST spectrum at India as evidence that LLST can explain mixed layer variability there. However, Mike and India are strikingly different from Papa in that their SST and SSS anomalies are nearly equally persistent, as evidenced by the way in which the normalized SST and SSS spectra overlap at all time scales. Although the total variances disagree (see figure caption), the spectra of SST and SSS for the model grid points nearest Mike and India exhibit this same qualitative behavior. As discussed in Sect. 1, if the local, linear stochastic mechanism were the only agent responsible for the variability, the decay time scales of SST and SSS would be different. Thus Figs. 10 and 11 indicate that the signatures of SST and SSS variations at these two weather stations are inconsistent with LLST.

Evidence of other mechanisms of variability is seen in the plots of the observed coherency between SST and SSS at these two weather stations, shown in Fig. 12. In contrast to the coherency on short time scales at Panulirus,

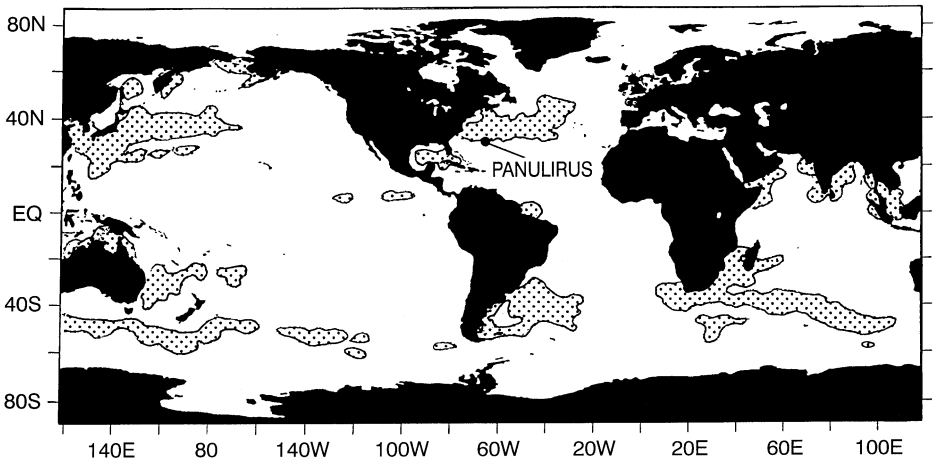

Fig. 8. *Shaded* regions indicate where rms sea level variability is greater than or equal to 12 cm, according to TOPEX altimeter data

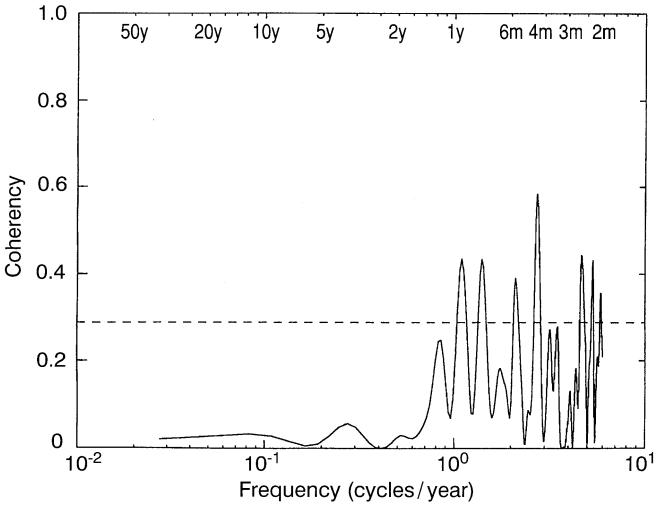

Fig. 9. The coherency of SST and SSS at weather station Panulirus. The *dashed horizontal line* shows the threshold below which 95% of the points would lie if the two time series were incoherent. Time scales are shown on the upper edge of the plot. The cross spectral statistics were calculated by taking the Fourier transform of the cross-covariance function using a Parzen window with a maximum lag of 6 y

there is pronounced coherency of SST and SSS on long time scales at Mike and India. This is especially noticeable at India. The explanation for this phenomenon lies in the fact that the time mean temperature and salinity fields both increase from north to south. Large-scale temporal variability in the ocean circulation would therefore produce coherent salinity and temperature fluctuations at a given location. Long term variability in oceanic SST and SSS advection is a more plausible explanation for the observed coherency of SST and SSS than local stochastic forcing, since it is difficult to imagine that atmospheric energy and water flux forcings could be coherent on such long time scales. Perhaps these variations in the ocean circulation are related to irregular oscillations of the thermohaline circulation, such as those in the GFDL coupled model, analyzed by Delworth et al. (1993). This is suggested by the presence of a peak in the model spectra at

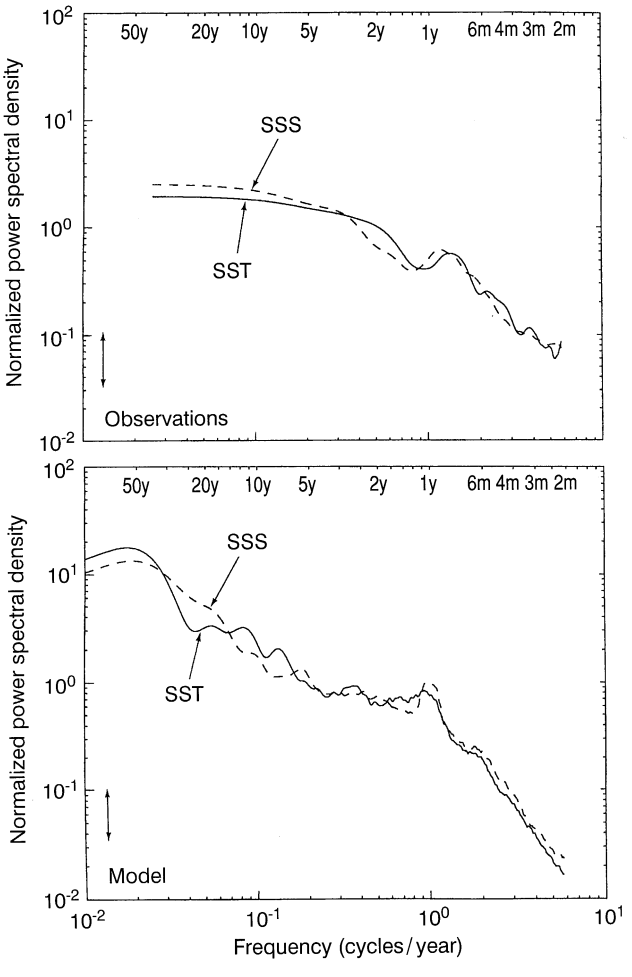

Fig. 10. As in Fig. 2, but for weather station Mike. The nearest model grid point is located at 65.2 °N, 1.9 °E. For the observations, the total variances used to normalize the autocovariance function were 0.00861 psu^2 for SSS and 0.285 (°C)^2 for SST. For the model, the total variances were 0.00146 psu^2 for SSS and 0.107 (°C)^2 for SST. The observed spectra are plotted out to the length of the time series (40.2 y for both SST and SSS)

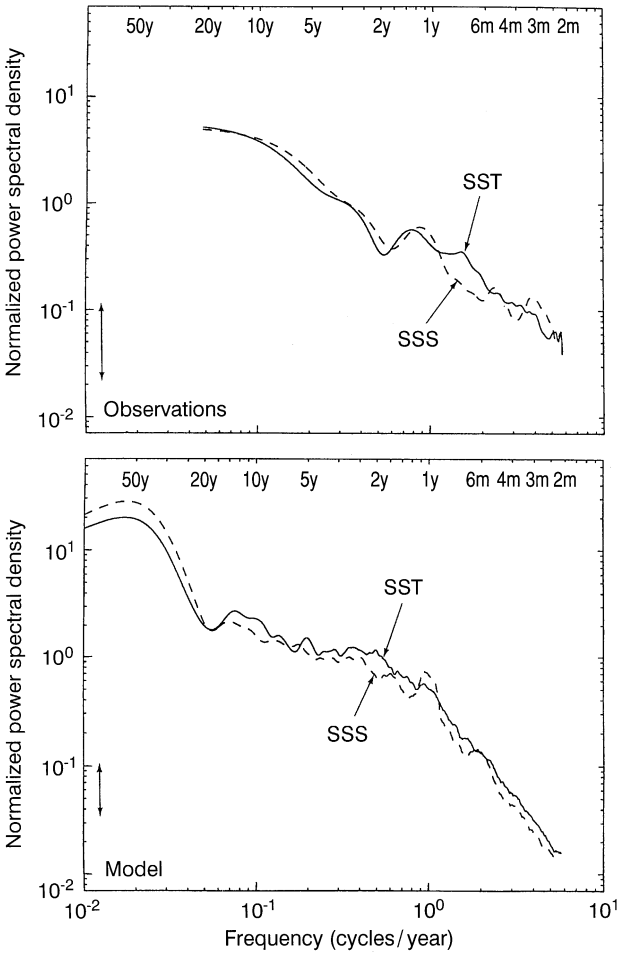

Fig. 11. As in Fig. 2, but for weather station India. The nearest model grid point is located at 60.8 °N, 20.6 °W. For the observations, the total variances used to normalize the autocovariance function were 0.00624 psu^2 for SSS and 0.406 (°C)^2 for SST. The observed spectra are plotted out to the length of the time series (25.3 y for both SST and SSS). For the model, the total variances were 0.00192 psu^2 for SSS and 0.146 (°C)^2 for SST. The observational SST spectrum presented here differs slightly from the spectrum presented in the Frankignoul and Hasselmann (1977) paper because the time series used in this study includes data from the post-1977 period

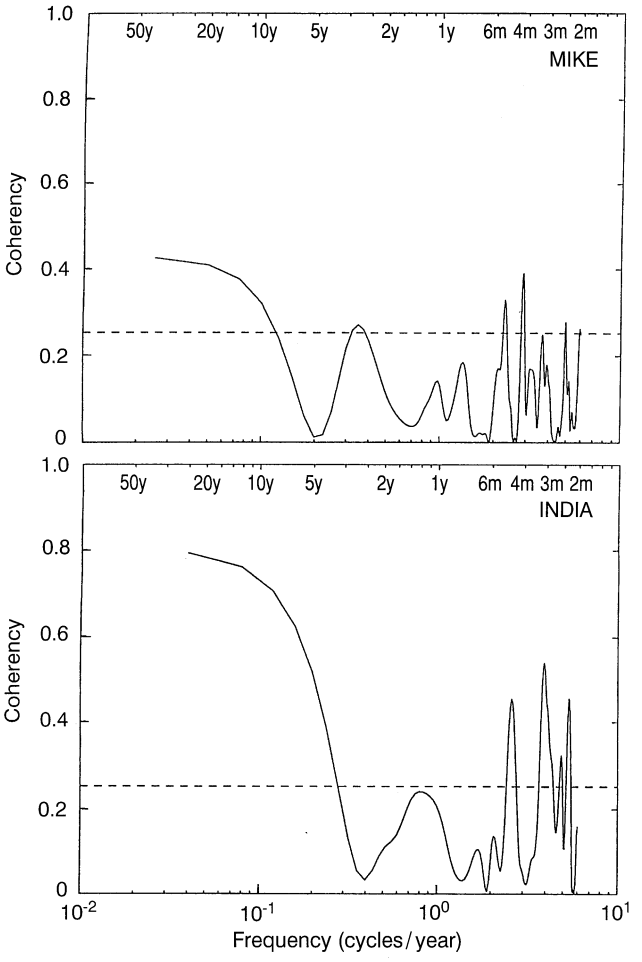

Fig. 12. The coherency of SST and SSS at weather stations Mike (*top*) and India (*bottom*). The *dashed horizontal line* shows the threshold below which 95% of the points would lie if the two time series were incoherent. Time scales are shown on the upper edge of the plot. The cross spectral statistics were calculated by taking the Fourier transform of the cross-covariance function using a Parzen window with a maximum lag of 72 (40) months for Mike (India)

50 y, which is the characteristic time scale of the model's thermohaline oscillation. The grid point nearest India is also located directly in the 'sinking region' of the model's thermohaline circulation and shows an especially strong peak at 50 y. In addition, the coherency plots of SST and SSS for the model grid points nearest India and Mike (not shown) closely resemble those shown in Fig. 12, with SST and SSS strongly coherent on these same long time scales. As with station Panulirus, the advection term in Eq. (1) may not be approximated by a damping term. At stations Mike and India, large-scale anomalies in the ocean's circulation make an important contribution to the forcing, rather than the damping, of local SST and SSS anomalies. Thus, in spite of the fact that the observed SST and SSS spectra resemble a red noise spectrum, it is not possible to invoke the local, linear stochastic mechanism to explain temperature or salinity variability at Mike and India, at least for long time scales. However, on short time scales, local stochastic forcing may be a more plausible explanation for the variability, as suggested by the goodness of the $1/\omega^2$ fit at high frequencies.

6 Summary and discussion

To summarize, results of spectral analysis of data at one of the weather stations and its corresponding model grid point are consistent with the local, linear stochastic picture. At Papa, in the northeast Pacific, the fact that the model and observational SSS spectra are redder than their SST counterparts conforms well to the predictions of LLST. Additional model results put LLST on an even firmer foundation at this location. The coherency between salinity's 'residual noise' time series and the water flux time series is significant at all time scales, indicating that the water flux is responsible for much of SSS variability. The frequency dependence of the coherency between the total energy flux and temperature's 'residual noise' time series is also close to what LLST predicts.

At the other three weather stations, LLST alone cannot adequately explain mixed-layer variability. At station Panulirus, mesoscale eddies, which are not resolved by the coupled model, enhance the variability at high frequencies. This is evidenced by the higher level of power spectral density at time scales less than one year in the observational record relative to the model grid point nearest Panulirus. In addition, observational SST and SSS exhibit significant coherency on these same time scales, indicating the passage of saline, warm-core or fresh, cold-core eddies. At stations India and Mike, in the North Atlantic, large-scale variations of the ocean circulation are responsible for much of the low frequency variability, as evidenced by the high degree of coherency between SST and SSS on long time scales in both the model and observations. Moreover, spectral analysis shows there is little difference in the redness of the SST and SSS spectra at both of these weather stations and their nearest model grid points, contradicting the prediction of LLST.

The observational record of SST and SSS variability is only complete enough to evaluate LLST at a few locations. However, model results can extend this assessment to the entire ocean, if only qualitatively. The relative redness of the SST and SSS spectra emerges from the preceding discussion as a critical factor in determining whether or not the local, linear stochastic mechanism can explain mixed-layer variability. One way to measure this factor is to compare the autocorrelation functions of the two variables. The top half of Fig. 13 shows the coupled model's geographical distribution of the ratio of the lag one autocorrelation of annual mean SST to lag one autocorrelation of annual mean SSS. Values of this parameter much less than one indicate that SSS anomalies are more persistent than their SST counterparts. Shaded areas show where the ratio exceeds 0.85, indicating approximately equal or greater persistence of SST compared to SSS. Thus in these regions, a key prediction of LLST is called into question.

Another critical factor in determining the relevance of LLST is the coherency between SST and SSS. The model cannot resolve mesoscale eddies, whose signature includes coherency between SST and SSS on short time scales at station Panulirus. However, the model can resolve large-scale variability of the ocean circulation. The coherency between SST and SSS sampled at long time scales reveals the regions of the model ocean where large-scale SST and SSS advection dominate mixed-layer variability. The shaded regions in the bottom half of Fig. 13 show where the coherency sampled at the 50 year time scale exceeds 0.5 (analogous to a correlation coefficient of 0.71).

Over most of the world ocean, SST and SSS are incoherent and SSS is redder than SST, signatures that are consistent with the local, linear stochastic mechanism. However, three regions run counter to this pattern in both of the plots of Fig. 13: the northern North Atlantic, nearly the entire southern ocean south of 45 °S, and the Sea of Okhotsk. The northern North Atlantic has been discussed already; the coherent variations in SST and SSS advection

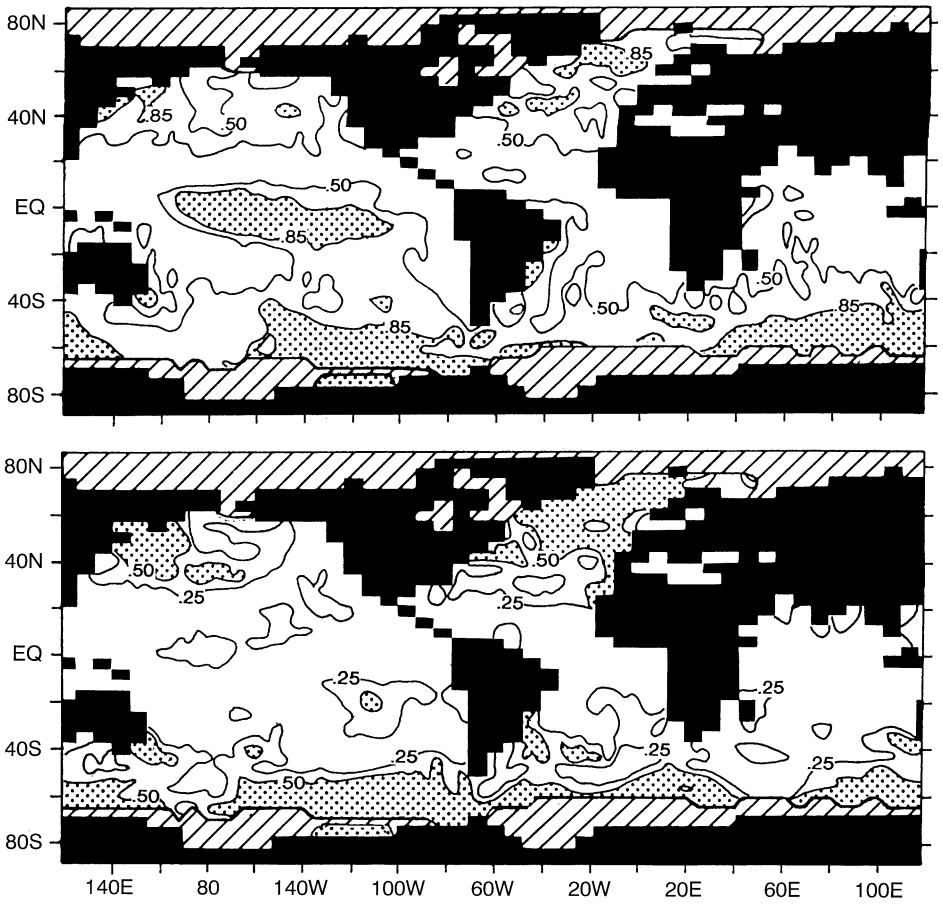

Fig. 13. *Top*: *shaded* regions show where the ratio of lag one autocorrelation of annual mean SST to lag one autocorrelation of annual mean SSS is greater than 0.85 for the coupled model. The 0.5 contour is also shown for comparison. *Bottom*: *shaded* regions show where the coherency between SST and SSS exceeds 0.5 on the 50 y time scale. The 0.25 contour is also shown for comparison. The cross spectral statistics were calculated by taking the Fourier transform of the cross-covariance function using a Parzen window with a maximum lag of 117 y. Regions covered by sea ice for an average of 2 months or more per year (as simulated by the model) are marked by diagonal lines

are related to oscillations in the thermohaline circulation. It is significant that two areas of the North Atlantic stand out in the top panel of Fig. 13. The southern-most area, directly south of Greenland and east of Newfoundland, coincides with the sinking region of the model's thermohaline circulation. An analysis of the other area, just southeast of the coast of Greenland, indicates that SST and SSS variations, result from irregular oscillations in the southward East Greenland current. This current (reminiscent of 'great salinity anomalies') fluctuates coherently with the thermohaline circulation, but not in phase with it (Delworth et al. 1997). Thus, there are actually two distinct areas of the North Atlantic where low frequency variability is determined mainly by large-scale advection. Similarly, the circulation in the model southern ocean is known to exhibit irregular oscillations on a centennial time scale, which induce substantial SST and SSS variability. In fact, the geographical distribution of coherency on the 100 year time scale (not shown) reveals that SST and SSS in the southern ocean are even more strongly coherent on the centennial time scale than the 50 year time scale. These fluctuations of surface conditions appear to be associated with the very gradual change of deep vertical velocity which, in turn, affects the meridional advection of the cold and fresh surface layer. Large-scale fluctuations of the ocean circulation therefore play an important role in the low frequency SST and SSS variability in both of these high-latitude regions.

These results are consistent with Manabe and Stouffer's (1996) analysis of SST variability (see Sect. 5 of that paper). They analyzed the same 1000-year run of the coupled model as well as the integration of a mixed-layer model that has the same atmosphere as the coupled model but a fixed depth mixed-layer with no ocean dynamics. This mixed layer is therefore forced solely by the model's atmosphere. Comparison of these two models can be used to shed light on the effects of ocean circulation on variability. At a high-latitude location (69.75 °N, 22.5 °W) in the North Atlantic, where SST and SSS are coherent and equally persistent according to Fig. 13, they compared the SST spectra of the coupled and mixed-layer models. While the power spectral density is similar at high frequencies, at periods longer than 20 years the power spectral density in the coupled model is more than one order of magnitude larger than the mixed layer model. They obtained similar results for a southern ocean location (60.75 °S, 142.5 °W) where SST and SSS are also coherent and equally persistent. This constitutes additional evidence that variations in oceanic heat advection in the coupled model have a huge impact on low frequency SST variability in these high latitude regions. Of course, it is possible that these variations in the ocean circulation are themselves induced by stochastic atmospheric forcing over the entire ocean. Some studies have examined the non-local, non-linear response of the ocean to stochastic forcing. Mikolajewicz and Maier-Reimer (1990) forced an ocean-only model with a white-noise freshwater flux and were able to induce a 320 year oscillation associated with the model's thermohaline circulation. Similar results were obtained from an ocean model forced by stochastically varying windstress, heat and water fluxes (Mikolajewicz and Maier-Reimer 1994). If these results can be extended to the real ocean, then the low-frequency variability at weather stations India and Mike, and at high latitudes in general, may be understood under the rubric of a stochastic theory that includes non-linear, non-local effects.

The equatorial Pacific also stands out in the plot of the ratio of lag one SST to lag one SSS, though not in the accompanying coherency plot. The model's SST anomalies are actually much more persistent than its SSS anomalies in this area of the ocean. Although not apparent from Fig. 13, the lag one autocorrelation of SST is more than twice as large as its SSS counterpart over much of this region, making the ratio of the two larger than anywhere else in the model ocean. This region is therefore very unusual. In-depth analysis of the equatorial Pacific is beyond the scope of this study; however, the model produces as well-documented phenomenon resembling the delayed-oscillator mode of ENSO (see Knutson and Manabe 1994; Knutson et al. 1996). This oscillation induces large changes in SST in the equatorial Pacific on a two to seven year time scale, which may enhance the persistence of SST relative to SSS. In addition, this region is unusual for its intense upwelling, which certainly affects both SST and SSS. In any case, it is unlikely that LLST is applicable in the equatorial Pacific for either the model or the real world. In this region, complex air-sea feedbacks dominate the variability, and the ocean certainly does not respond passively to atmospheric forcing.

This still leaves large portions of the world ocean where LLST may be appropriate, as all available evidence shows at weather station Papa. Reynolds (1978) showed that the spectrum of SST at all locations in a broad region of the central Pacific could best be characterized as a red noise spectrum. Although by itself not conclusive evidence that the local, linear stochastic mechanism is operating, additional model results from Manabe and Stouffer (1996) suggest that LLST may be relevant for this and other areas of the world ocean. First, they showed that the coupled model's SST spectrum averaged over mid-latitude oceanic boxes in the North Pacific and Atlantic is nearly a perfect red noise spectrum in accordance with Reynold's observational result. In addition, the SST spectrum averaged over the same regions in a mixed-layer model is nearly in perfect agreement with the corresponding coupled model result at all frequencies. This indicates that in these regions, variations in the ocean circulation play a subordinate role to the atmosphere in the forcing of the coupled model's SST anomalies.

Joint analysis of both salinity and temperature reveals a great deal about the mechanisms of variability at the sea surface. With results from this and preceding sections in hand, it is now possible to identify qualitatively the regions of the world ocean where LLST probably does and does not apply. As illustrated in Sect. 5.2 mesoscale eddies can contribute significantly to SST and SSS variability on time scales less than one year. Areas outlined with a heavy contour in Fig. 14 represent regions where the monthly mean rms sea level variability is at least as large as that at Panulirus (12 cm), indicating the presence of mesoscale eddies. Of course, this is only a qualitative measure of eddy activity, but it is a useful guide nonetheless. In these regions, associated mainly with boundary currents and the intense circumpolar current, there is probably

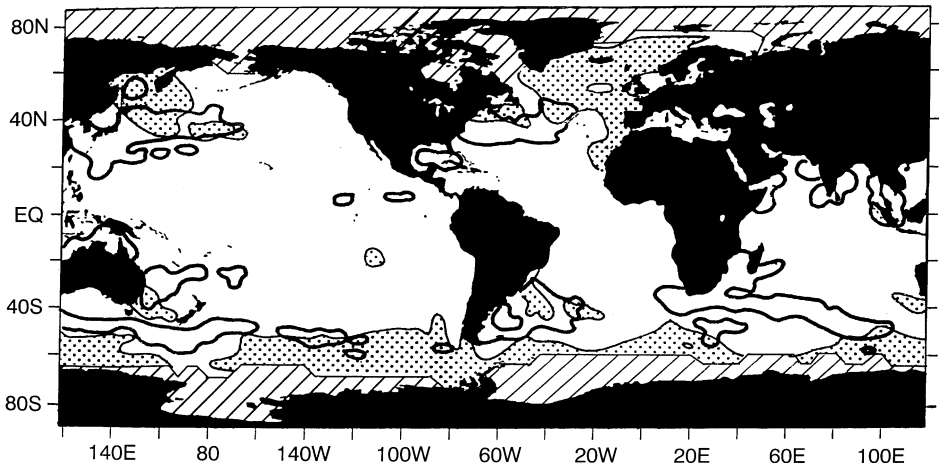

Fig. 14. Regions where LLST may not apply. Areas outlined with a *heavy contour* represent regions where the rms sea level variability is equal to, or exceeds that at Panulirus (12 cm), according to TOPEX altimeter data. The areas where the model coherency exceeds 0.5 on the 50-y time scale are *shaded*. Regions covered by sea ice for an average of 2 months or more per year (as simulated by the model) are marked by diagonal lines

enhanced variability on short time scales. This makes the SST and SSS spectra 'whiter' than if the local, linear stochastic mechanism alone were operating. This view is consistent with the work of Reynolds (1978), who showed that in the region of the Kuroshio current, the Langevin equation is not the best statistical model for SST variability. Also shown in Fig. 14 are the model results from the bottom half of Fig. 13: regions where the coherency exceeds 0.5 on the 50 y time scale are shaded. These coherent fluctuations of SST and SSS indicate that large-scale oceanic advection is forcing local low frequency SST and SSS anomalies. Thus the outlined and shaded regions in Fig. 14 together show where local stochastic atmospheric forcing cannot be the only cause of SST and SSS variability. Here, both large-scale and mesoscale oceanic processes must be taken into account. Outside of these regions, with the exception of the equatorial Pacific, the local linear version of stochastic theory may be applicable.

Acknowledgements. We thank Kirk Bryan, Tom Delworth, Steve Griffies, Anand Gnanadesikan, Yoshio Hayashi, Isaac Held and Tapio Schneider for many useful discussions. Also, we thank Ron Stouffer for providing the results from the 1 000 year integration of the GFDL coupled model. Gilles Reverdin was very generous in sharing his collection of North Atlantic SST and SSS data. Finally, we thank Klaus Hasselmann and one anonymous reviewer for their many valuable comments. Figure 8 was derived from a plot provided by the CNES (French Space Agency) AVISO project through the WWW server 'http: //www-aviso.cls.cnes.fr'

References

Alexander MA, Penland C (1996) Variability in a mixed layer ocean model driven by stochastic atmospheric forcing. J Clim 9: 2424–2442

Bryan K (1969) Climate and the ocean circulation: III. The ocean model. Mon Weather Rev 97: 806–827

Bryan K, Lewis L (1979) A water mass model of the world ocean. J Geophys Res 84(C5): 2503–2517

Delworth T, Manabe S, Stouffer RJ (1993) Interdecadal variations of the thermohaline circulation in a coupled ocean-atmosphere model. J Clim 16: 1993–2011

Delworth T, Manabe S, Stouffer RJ (1997) Multidecadal climate variability in the Greenland Sea and surrounding regions: a coupled model simulation. GRL (in press)

Frankignoul C (1981) Low-frequency temperature fluctuations off Bermuda. J Geophys Res 86(C7): 6522–6528

Frankignoul C, Hasselmann K (1977) Stochastic climate models, Part II: application to sea-surface temperature anomalies and thermocline variability. Tellus 29: 289–305

Gordon CT, Stern W (1982) A description of the GFDL Global Spectral Model. Mon Weather Rev 110: 625–644

Hasselmann K (1976) Stochastic climate models, Part I: theory. Tellus 28: 473–485

Julian P (1975) Comments on the determination of significance levels of the coherence statistic. J Atmos Sci 32: 836–837

Knutson T, Manabe S (1994) Impact of increased CO_2 on simulated ENSO-like phenomena. Geophys Res Let 21: 2295–2298

Knutson T, Manabe S (1996) Simulated ENSO in a global coupled ocean-atmosphere model: multi-decadal amplitude modulation and CO_2 sensitivity. J Clim (in press)

Levitus S (1982) Climatological Atlas of the World Ocean, Prof Pap 13. National Oceanic and Atmospheric Administration

Manabe S, Hahn D (1981) Simulation of atmospheric variability. Mon Weather Rev 109: 2260–2286

Manabe S, Stouffer RJ (1996) Low frequency variability of surface air temperature in a 1 000 year integration of a coupled ocean-atmosphere model. J Clim 9: 376–393

Manabe S, Stouffer RJ, Spelman M, Bryan K (1991) Transient responses of a coupled ocean-atmosphere model to gradual changes of atmospheric CO_2. Part I: annual mean response. J Clim 4: 785–817

Marotzke J, Stone P (1995) Atmospheric transports, the thermohaline circulation, and flux adjustments in a simple coupled model. J Phys Oceanogr 25: 1350–1364

Mikolajewicz U, Maier-Reimer E (1994) Mixed boundary conditions in ocean general circulation models and their influence on the stability of the model's conveyor belt. J Geophys Res 99: 22633–22644

Mikolajewicz U, Maier-Reimer E (1990) Internal secular variability in an ocean general circulation model. Clim Dyn 4: 145–156

Oort A, Anderson L, Peixoto J (1994) Estimate of the energy cycle of the oceans. J Geophys Res 99(C4): 7665–7688

Orszag SA (1970) Transform method for calculating vector-coupled sums: application to the spectral form of the vorticity equation. J Atmos Sci 27: 890–895

Redi MH (1982) Oceanic isopycnal mixing by coordinate rotation. J Phys Oceanogr 12: 1154–1158

Reynolds R (1978) Sea surface temperature anomalies in the North Pacific Ocean. Tellus 30: 97–103

Robinson AR (1983) Eddies in marine science. Springer, Berlin Heidelberg New York Tokyo, pp 21–41

Tziperman E, Bryan K (1993) Estimating global air-sea fluxes from surface properties and from climatological flux data using an oceanic general circulation model. J Geophys Res 98(C12): 22629–22644